Sixth Asia-Pacific Symposium on Engineering Plasticity and Its Applications, 2nd-6th December 2002, Sydney, NSW, Australia, Trans. Tech., pp. 827-834.

Thermo-Mechanical Finite Element Model of Shell Behavior In The Continuous Casting of Steel

Chunsheng Li and Brian G. Thomas [1]

[1] Department of Mechanical & industrial Engineering

University of Illinois at Urbana-Champaign

1206 W. Green St., Urbana, IL 61801, USA

Keywords: Continuous Casting, Finite Element Method, Solidification, Elastic-viscoplasticity, Hot Tear, Crack criterion, 2D Generalized Plane Strain, Bulging, Thermal Stress Model.

Abstract. A finite-element model, CON2D, has been developed to simulate temperature, stress, and shape development during the continuous casting of steel, both in and below the mold. The stress model features an elastic-viscoplastic creep constitutive equation that accounts for the different responses of the liquid, semi-solid, delta-ferrite, and austenite phases. Temperature and composition-dependent functions are also employed for properties such as thermal linear expansion. A contact algorithm is developed to prevent penetration of the shell into the mold wall due to the internal liquid pressure. An efficient two-step algorithm has been developed to integrate these highly non-linear equations. An inelastic strain damage criterion is developed to predict hot tear crack formation, which includes the contribution of pseudo-strain due to the flow of the liquid during feeding of the mushy zone. The model is validated with an analytical solution for both temperature and stress in a solidifying slab. It is then applied to predict the maximum casting speed to avoid crack formation due to bulging below the mold during casting of steel billets.

Introduction

Computational models are important tools to study the complex process of continuous casting of steel. They can help to understand how defects form and to optimize casting conditions to maximize quality and productivity at low cost. Brimacombe and coworkers applied both heat flow [1] and stress models [2] to study crack formation in slabs. Kristiansson [3] applied a thermal stress model of square billets that featured time-dependent plasticity. Recently, Fachinotti *et. al.* developed a mixed Eulerian-Lagrangian [4] thermal mechanical model to study round steel billets.

A thermal-mechanical finite element model, CON2D, has been developed at the University of Illinois over the past decade [5, 6]. This paper summarizes the features of this model and describes one of its recent applications: prediction of the maximum casting speed to avoid crack formation due to bulging below the mold during continuous casting of square billets.

Heat Transfer and Solidification Model

The model solves a 2D finite-element discretization of the transient heat conduction equation in a Lagrangian reference frame that moves down through the caster with the solidifying steel shell. The nonlinear enthalpy gradients that accompany latent heat evolution were handled using a spatial averaging method by Lemon [7]. It adopts a three-level time-stepping method by Dupont [8].

Stress Model

The force equilibrium, constitutive, and strain displacement equations in this 2-D slice through the shell are solved under a condition of generalized plane strain in the casting direction [5].

The total strain increment, $\{\Delta\varepsilon\}$, is composed of elastic, $\{\Delta\varepsilon_e\}$, thermal, $\{\Delta\varepsilon_{th}\}$, inelastic strain, $\{\Delta\varepsilon_{in}\}$, and flow strain, $\{\Delta\varepsilon_{flow}\}$, components. Thermal strain due to volume changes caused by both temperature differences and phase transformations is calculated from the thermal linear expansion (TLE) of the material, which is based on density measurements.

$$\{\varepsilon_{th}\} = (TLE(T) - TLE(T_0))\{1 \quad 1 \quad 0 \quad 1\}^T \quad where \quad TLE(T) = \sqrt[3]{\rho(T_0)/\rho(T)} - 1 \tag{1}$$

A unified constitutive model is used here to capture the temperature- and strain-rate sensitivity of high temperature steel. The instantaneous equivalent inelastic strain rate $\dot{\bar{\varepsilon}}_{in}$ is adopted as the scalar state function, which depends on the current equivalent stress, $\bar{\sigma}$, temperature, T, the current equivalent inelastic strain, $\bar{\varepsilon}_{in}$, which accumulates below the solidus temperature, and carbon content of the steel. When the steel is mainly austenite phase, (%γ >90%), Model III by Kozlowski [9] was applied. This function matches tensile test measurements of Wray [10] and creep test data of Suzuki [11]. When the steel contains significant amounts of soft delta-ferrite phase (%δ >10%), a power-law model is used, which matches measurements of Wray above 1400 ^{o}C [12]. Fig. 1 shows the accuracy of the constitutive model predictions compared with stresses measured by Wray [13] at 5% strain at different strain rates and temperatures. This figure also shows the higher relative strength of austenite, which is important for stress development in the solidifying shell discussed later. The standard von Mises loading surface, associated plasticity and normality hypotheses in the Prandtl-Reuss flow law is applied to model isotropic hardening of these plain carbon steels [14].

As a fixed-grid approach is employed, liquid elements are generally given no special treatment regarding material properties or finite element assembly. To enforce negligible shear stress in the liquid, the following constitutive equation is used to provide an extremely rapid creep strain rate in every element containing any liquid, (*ie.*, $T > T_{solidus}$).

$$\dot{\bar{\varepsilon}}_{flow} = \begin{cases} 10^8 \left(|\bar{\sigma}| - \sigma_{yield} \right)^5 & |\bar{\sigma}| > \sigma_{yield} \\ 0 & |\bar{\sigma}| \le \sigma_{yield} \end{cases} \quad where \quad \sigma_{yield} = 0.01 MPa \tag{2}$$

The same Prandtl-Reuss relation used for the solid is adopted to expand this scalar strain rate to its multi-dimensional vector. This fixed-grid approach avoids difficulties of adaptive meshing and allows strain to accumulate in the mushy region, which is important for the prediction of hot tear cracks. As in the real system, the total mass of the liquid domain is not constant, and the inelastic strain accumulated in the liquid region represents mass transport due to fluid flow in and out of the domain, so is denoted as "flow strain". Positive flow strain indicates fluid feeding into the simulated region.

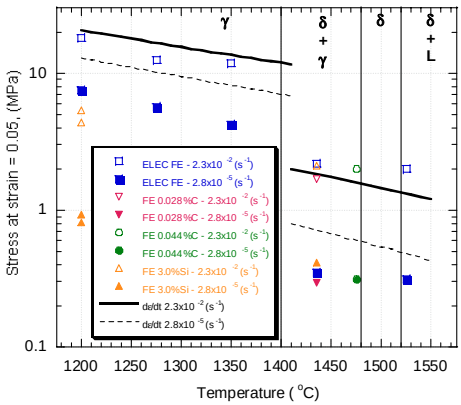

Figure 1: Comparison of predicted and measured stress [13]

Finite Element Implementation. Applying the standard Galerkin's method to the governing equations gives the linear algebraic equations to solve for temperature and then displacement within each time step. The stress model

uses 6-node quadratic-displacement triangle elements, which were each divided into four 3-node linear-temperature elements for the heat transfer calculation. The stress calculation involves force vectors due to increments of thermal and inelastic strain, ferrostatic pressure and shell/mold interaction at certain internal boundaries, and elastic strain corrections from the previous time step.

$$[K]\{\Delta u\}^{t+\Delta t} = \left\{\Delta F_{\varepsilon_{th}}\right\}^{t+\Delta t} + \left\{\Delta F_{\varepsilon_{pl}}\right\}^{t+\Delta t} + \left\{F_{fp}\right\}^{t+\Delta t} + \left\{F_{el}\right\}^{t+\Delta t} \tag{3}$$

Integration of the Constitutive Model. The highly strain-rate-dependent constitutive models involved in this solidification problem require a robust numerical integration technique to avoid numerical difficulties. This work applies a "local-global" method that alternates in each time step between implicit time integration of the constitutive equations to accurately estimate the future stress at each Gauss point, followed by standard finite element spatial integration. Specifically, the integration procedure used within each time step is summarized as:

1. Estimate $\{\Delta\hat{\varepsilon}\}$ based on $\{\Delta u\}$ from the previous time step: $\{\Delta\hat{\varepsilon}\} = [B]\{\Delta u\}^t$.

2. Calculate $\{\sigma^*\}^{t+\Delta t}$, $\bar{\sigma}^*$ and $\{\sigma^{*\prime}\}^{t+\Delta t}$, needed to define the direction of the stress vector.

$$\{\sigma^*\}^{t+\Delta t} = [D]^{t+\Delta t}\left(\{\varepsilon\}^t - \{\varepsilon_{th}\}^t - \{\varepsilon_{in}\}^t + \{\Delta\hat{\varepsilon}\} - \dot{\varepsilon}_{th}^{t+\Delta t}\Delta t\{1 \quad 1 \quad 0 \quad 1\}^T\right) \tag{4}$$

3. Solve the following two ordinary differential equations simultaneously for $\bar{\varepsilon}_{in}^{t+\Delta t}$ and $\bar{\hat{\sigma}}^{t+\Delta t}$ at each local Gauss point, using a fully implicit bounded Newton-Raphson integration method from Lush [15]. This method gives the best robustness and efficiency of several alternative approaches evaluated [6]. Function F is either Kozlowski model III for γ, the power law for δ, or flow strain for liquid phase.

$$\begin{aligned}
\bar{\varepsilon}_{in}^{t+\Delta t} &= \bar{\varepsilon}_{in}^{t} + F\left(T, \bar{\hat{\sigma}}^{t+\Delta t}, \bar{\varepsilon}_{in}^{t+\Delta t}, \%C\right)\Delta t \\
\bar{\hat{\sigma}}^{t+\Delta t} &= \bar{\sigma}^{*t+\Delta t} - 3\mu^{t+\Delta t} F\left(T, \bar{\hat{\sigma}}^{t+\Delta t}, \bar{\varepsilon}_{in}^{t+\Delta t}, \%C\right)\Delta t
\end{aligned} \tag{5}$$

4. Expand this scalar stress estimate into vector form[1]: $\{\hat{\sigma}\}^{t+\Delta t} = \bar{\hat{\sigma}}^{t+\Delta t}\dfrac{\{\sigma^{*\prime}\}^{t+\Delta t}}{\bar{\sigma}^{*t+\Delta t}} + \dfrac{1}{3}\sigma_m^{*t+\Delta t}\{\delta\}^T$.

5. Calculate $\dot{\bar{\varepsilon}}_{in}^{t+\Delta t}$ from $\bar{\hat{\sigma}}^{t+\Delta t}$ and $\bar{\varepsilon}_{in}^{t+\Delta t}$ using F according to the material phase.

6. Expand this scalar inelastic strain estimate into a vector $\{\dot{\varepsilon}_{in}\}^{t+\Delta t}$ with the same direction as $\{\hat{\sigma}'\}^{t+\Delta t}$ using Prandtl-Reuss eqs.; Update $\{\varepsilon_{in}\}^{t+\Delta t} = \{\varepsilon_{in}\}^t + \{\dot{\varepsilon}_{in}\}^{t+\Delta t}\Delta t$ only for solidified elements.

7. Use classic FEM spatial integration to solve Eq. 6 for $\{\Delta u\}^{t+\Delta t}$ based on $\{\hat{\sigma}\}^{t+\Delta t}$ and $\{\dot{\varepsilon}_{in}\}^{t+\Delta t}$.

8. Finally, find $\{\Delta\varepsilon\}^{t+\Delta t}$ from $\{\Delta u\}^{t+\Delta t}$ and update $\{\varepsilon\}^{t+\Delta t}$ and $\{\sigma\}^{t+\Delta t}$.

[1] $\{\sigma^{*\prime}\}^{t+\Delta t} = \{\sigma^*\}^{t+\Delta t} - \dfrac{1}{3}\sigma_m^{*t+\Delta t}\{\delta\}^T$; $\sigma_m^{*t+\Delta t} = \sigma_x^{*t+\Delta t} + \sigma_y^{*t+\Delta t} + \sigma_z^{*t+\Delta t}$; $\{\delta\} = \{1 \quad 1 \quad 0 \quad 1\}$

Ferrostatic Pressure. Ferrostatic pressure due to gravity acting on the internal liquid pool, $F_p = \rho g z$, is applied as an internal boundary condition. Each three-node element containing exactly two nodes just below the solidus temperature is subjected to a load pushing toward the mold wall.

Mold Wall Constraint. The mold wall provides support to the solidifying shell before it reaches the mold exit. A proper mold wall constraint is needed to prevent the solidifying shell from penetrating the mold wall, but allowing the shell to shrink freely. The present method developed by Moitra [5, 16] is based on penalty method. It allows the shell deform freely at the beginning of each step and repeatedly constraint half of the penetrating nodes until no penetration occur.

Failure Criterion. A simple empirical critical strain function, ε_c, fitted by Won [17] from many measurements, was adopted in this work as a fracture criterion given in Eq. 6. Hot tear cracks form if the thick dendrites in the brittle temperature range, ΔT_B [17], prevent the surrounding liquid to compensate the contraction of interdendritic liquid and solid expansion. Cracks are predicted when damage strain, ε_{damage}, exceeds the critical strain, ε_c.

$$\varepsilon_{damage} \geq \varepsilon_c \quad where \quad \varepsilon_{damage} = \sum_{f_s=0.9}^{f_s=0.99} \Delta\varepsilon_{flow\_hoop} \quad and \quad \varepsilon_c = \frac{0.02821}{\dot{\varepsilon}^{0.3131} \Delta T_B^{\,0.8638}} \tag{6}$$

Damage strain is defined as the flow strain accumulated within the brittle temperature range, calculated during the post-processing phase. The damage strain component chosen for comparison is taken perpendicular to the dendrite growth direction, which is along the "hoop" direction, so named because it is tangential to the surface of the solidifying shell.

Model Validation

An analytical solution of thermal stresses in an unconstrained solidifying plate developed by Weiner and Boley [18] is used as a validation problem for this solidification stress model. The elastic-perfectly-plastic constitutive equation used in this solution was transformed to a numerically challenging problem of the form in Eq. 2 and computed by CON2D.

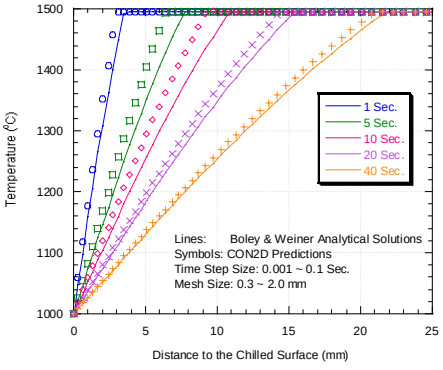

Figure 2: Temperatures through Solidifying Plate at Different Solidification Times

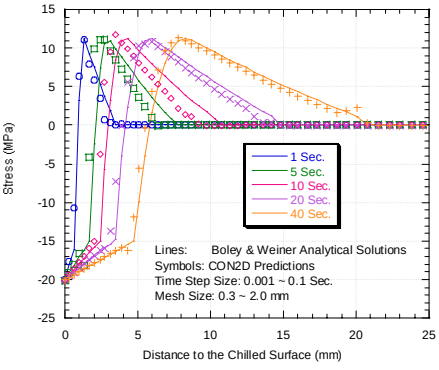

Figure 3: Stresses through Solidifying Plate at Different Solidification Times

Figs. 2 and 3 show the analytical solutions computed with MATLAB [19]. The CON2D results match within 2% average error with the same mesh and time step sizes used in the actual 2-D analyses in Table 2. This demonstrates that the model is numerically consistent and has an acceptable mesh.

Table 1: Material Details in Billet Analysis

Table 2: Simulation Conditions

Steel Composition (wt%)	0.27C, 1.52Mn, 0.34Si, 0.015S, 0.012P	Billet Section Size (mm×mm)	**120×120**
		Total Mold Length (mm)	**800**
		Mesh Size (mm×mm)	0.1×0.1~1.4×1.0
Liquidus Temp. (^{o}C)	1500.72	Number of Nodes	**7381**
70% Solid Temp. (^{o}C)	1477.02	Number of Elements	**7200**
90% Solid Temp. (^{o}C)	1459.90	Time Step Size (sec.)	0.001 - 0.5
Solidus Temp. (^{o}C)	1411.79	Pouring Temperature (^{o}C)	1540.0

Application to Thermal Mechanical Behavior of Continuous-Cast Billet

The finite-element thermal-mechanical model is next applied to predict temperature, bulging, strain, stress and fracture in continuous cast steel billets, in the absence of any sub-mould support. The results are then used to find the critical casting speeds to avoid quality problems related to bulging below the mold.

Modeling Domain. The model domain is a L-shaped region in one quarter of a transverse section through the billet, as shown in Fig. 4. Assuming two-fold symmetry and taking out the center portion of the section, which is always liquid, saves computational cost.

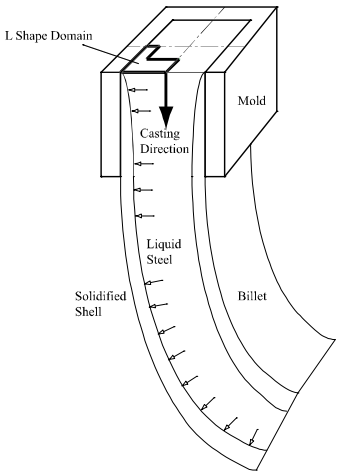

Figure 4: Modeling Domain

Heat Flux at Shell Surface. The instantaneous heat flux, given in Eq. 7, is based on fitting many plant measurements [20]. It is assumed to be uniform around the perimeter of the billet surface in order to simulate ideal taper and perfect contact between the shell and mold. After the billet leaves the mold, its surface temperature is kept unchanged from its circumferential profile at mold exit. This eliminates the effect of spray cooling practice on sub-mold reheating or cooling and the associated complication for the stress/strain development. Transformation temperatures defining the phase evolution of the typical plain carbon steel studied here are given in Table 1.

$$q\left(MW/m^2\right)=\begin{cases}5-0.2444t\left(\sec.\right) & t\le 1.0\sec.\\ 4.7556t\left(\sec.\right)^{-0.504} & t>1.0\sec.\end{cases} \tag{7}$$

Simulation Results. The model is used to simulate the mechanical behavior of a steel billet under the conditions shown in Table 2 with various casting speeds.

Figs. 5(a) and 6(a) show the distorted temperature contours at 200mm below the mold exit for the important casting speeds of 2.2m/min and 5.0m/min, respectively. The first speed is a typical casting speed, while the second speed is the critical speed at which hot tear crack failure of the shell is just predicted to occur. The shell is hotter and thinner at the higher casting speed, owing to less time in the mold. This thinner, hotter, and weaker shell then bulges more under the ferrostatic pressure below the mold.

Figs. 5(b) and 6(b) show contours of hoop values of stress constructed by taking components in the x direction across the dendrites in the horizontal portion of the domain and the y direction in the vertical portion. High values appear at the off-corner sub-surface region, due to a hinging effect that

the ferrostatic pressure over the entire face exerts around the corner. This bends the shell around the corner and generates high subsurface tensile stress at the weak solidification front in the off-corner subsurface location. This tensile stress increases at higher casting speed. There is no obvious high stress region at the low casting speed. Surface hoop stress is compressive at low casting speed. This indicates no possibility of surface cracking. However, tensile surface hoop stress is generated below the mold at high speed in Fig. 6(b) at the face center due to excessive bulging. This tensile stress and strain might contribute to surface longitudinal corner cracks.

Figs. 5(c) and 6(c) show contours of damage strain accumulated according to Eq. 6. The highest values of damage strain appear at the off-corner sub-surface region in the hoop direction. Moreover, significantly higher values are found for the higher casting speed case. At 5.0 m/min casting speed, the damage strain in the hoop direction exceeds the damage threshold [17] at 12 nodes, all located near the off-corner subsurface region. This is caused by the hinging mechanism around the corner. No nodes fail at 2.2m/min casting speed or at the center surface.

The effect of mold length and section size on the critical casting speed is discussed elsewhere [20]. The critical casting speed predictions match industrial experience.

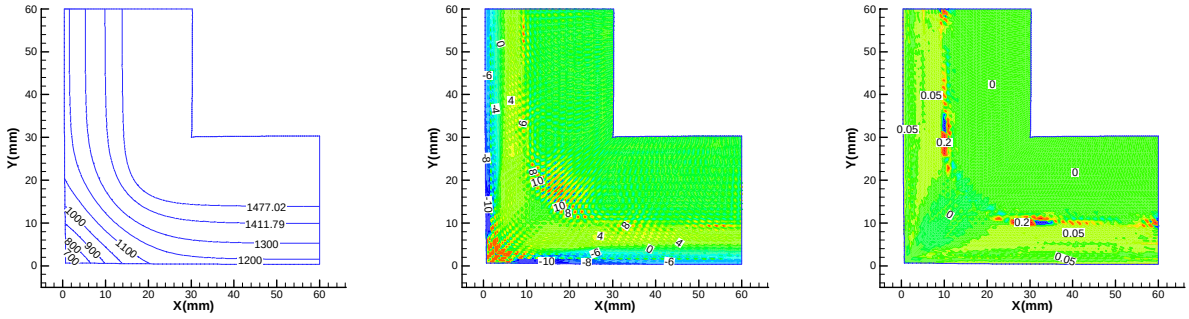

(a) Temperature (b) Hoop Stress (c) Damage Strain

Figure 5: Distorted Contours at 200mm below Mold Exit for the Casting Speed of **2.2m/min**

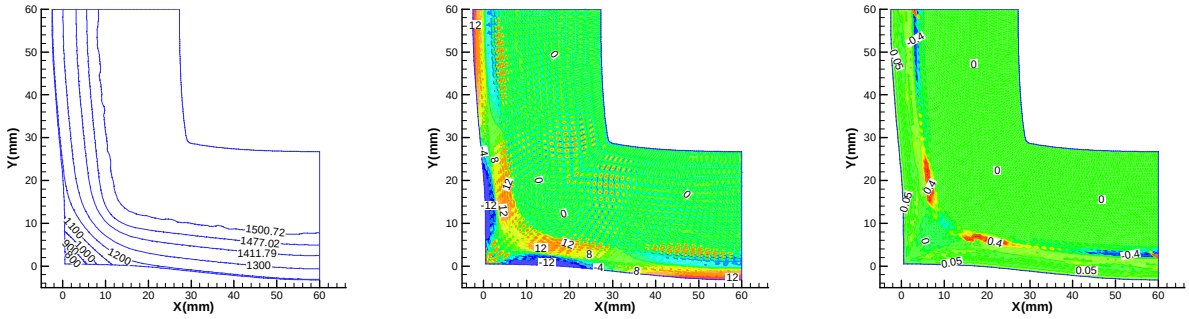

(a) Temperature (b) Hoop Stress (c) Damage Strain

Figure 6: Distorted Contours at 200mm below Mold Exit for the Casting Speed of **5.0m/min**

Conclusions

A thermal-mechanical finite-element model, CON2D, has been developed to analyze the temperature, stress and strain distribution in the solidifying shell in the continuous casting of steel. This is a Lagrangian approach with a 2-D generalized plane strain condition, which gives a reasonable prediction of 3-D mechanical behavior by solving incremental equations within a horizontal slice domain. Unified elastic-viscoplastic constitutive models for both austenite and δ-

ferrite phases of the steel match tensile and creep test data. Liquid is treated by giving it a elastic-perfect-plastic constitutive model with small yield stress to prevent nonphysical high shear stress in the liquid. A robust and efficient time integration technique, alternating local-global method, is adopted to integrate the highly non-linear constitutive equations. An efficient contact algorithm enables proper treatment of the interaction between the mold wall and shell surface. Ferrostatic pressure from the liquid is taken into account through an internal boundary condition. An empirical hot tear fracture criterion is used to predict hot tear cracks quantitatively.

The model is validated by extensive comparison with an analytical solution for solidification stress. It is then applied to investigate the effect of casting speed during continuous casting of a square steel billet. If casting speed exceeds a critical threshold, then sub-surface, off-corner longitudinal hot tear cracks are predicted to form due to sub-mold bulging.

Acknowledgements

The authors thank the steel industry members of the Continuous Casting Consortium for their financial support of this project. Work by previous students, A. Moitra, H. Zhu, and J. Parkman, on the CON2D program is also gratefully acknowledged.

References

[1] A. Grill, K. Sorimachi and J. K. Brimacombe: *Metall. Trans. B*, (1976), **7B** (2), 177.

[2] K. Sorimachi and J. K. Brimacombe: *Ironmaking Steelmaking*, (1977), **4** (4), 240.

[3] J. O. Kristiansson: *J. Therm. Stresses*, (1982), **5** (3-4), 315.

[4] A. E. Huespe, A. Cardona and V. Fachinotti: *Computer Methods in Applied Mechanics & Engineering*, (2000), **182** (3-4), 439.

[5] A. Moitra: Ph.D. Thesis, University of Illinois at Urbana-Champaign, (1993).

[6] H. Zhu: Ph.D. Thesis, University of Illinois at Urbana-Champaign, (1996).

[7] E. Lemmon:, in Numerical Methods in Heat Transfer, **1**, R.W. Lewis, K. Morgan and O.C. Zienkiewicz, eds., John Wiley & Sons, (1981), 201-213.

[8] T. Dupont, G. Fairweather and J. P. Johnson: *SIAM Journal on Numerical Analysis*, (1974), **11** (2), 392.

[9] P. F. Kozlowski, B. G. Thomas, J. A. Azzi and H. Wang: *Metallurgical and Materials Transactions, A*, (1992), **23** (March), 903.

[10] P. J. Wray: *Metallurgical and Materials Transactions A*, (1982), **13A** (January), 125.

[11] T. Suzuki, K. H. Tacke, K. Wunnenberg and K. Schwerdtfeger: *Ironmaking and Steelmaking*, (1988), **15** (2), 90.

[12] B. G. Thomas and J. T. Parkman: *Thermec '97 International Conference on Thermomechanical Processing of Steel and Other Materials*, TMS, eds., TMS, Warrendale, PA, (1997)**, II**, 2279.

[13] P. J. Wray: *Metallurgical and Materials Transactions A*, (1976), **7A** (November), 1621.

[14] J. Lemaitre and J. L. Chaboche: *Mechanics of Solid Materials*, Cambridge University Press, (1990), 556.

[15] A. M. Lush, G. Weber and L. Anand: *International Journal of Plasticity*, (1989), **5**, 521.

[16] A. Moitra, B. G. Thomas and H. Zhu: *76th Steelmaking Conference*, ISS, eds., Warrendale, PA, (1993)**, 76**, 657.

[17] Y. Won, T.-J. YEO, D. SEOL and K. OH: *Metallurgical and Materials Transactions B*, (2000), **31B** (4), 779.

[18] J. H. Weiner and B. A. Boley: *J. Mech. Phys. Solids*, (1963), **11**, 145.

[19] The Mathworks. Inc.: *MATLAB User Manual, Ver. 5.3*, 3 Apple Hill Dr., Natick, MA 01760, (1999).

[20] C. Li and B. G. Thomas: *85th Steelmaking Conference*, ISS-AIME, eds., ISS-AIME, Warrendale, PA, (2002)**, 85**, 109.